BIOCHEMISTRY
including biophysical chemistry & molecular biology

Article

pubs.acs.org/biochemistry

Structure and Protein−Protein Interactions of Methanol Dehydrogenase from *Methylococcus capsulatus* (Bath)

Megen A. Culpepper and Amy C. Rosenzweig*

Departments of Molecular Biosciences and Chemistry, Northwestern University, Evanston, Illinois 60208, United States

Supporting Information

ABSTRACT: In the initial steps of their metabolic pathway, methanotrophic bacteria oxidize methane to methanol with methane monooxygenases (MMOs) and methanol to formaldehyde with methanol dehydrogenases (MDHs). Several lines of evidence suggest that the membrane-bound or particulate MMO (pMMO) and MDH interact to form a metabolic supercomplex. To further investigate the possible existence of such a supercomplex, native MDH from *Methylococcus capsulatus* (Bath) has been purified and characterized by size exclusion chromatography with multi-angle light scattering and X-ray crystallography. *M. capsulatus* (Bath) MDH is primarily a dimer in solution, although an oligomeric species with a molecular mass of ∼450−560 kDa forms at higher protein concentrations. The 2.57 Å resolution crystal structure reveals an overall fold and $\alpha_2\beta_2$ dimeric architecture similar to those of other MDH structures. In addition, biolayer interferometry studies demonstrate specific protein−protein interactions between MDH and *M. capsulatus* (Bath) pMMO as well as between MDH and the truncated recombinant periplasmic domains of *M. capsulatus* (Bath) pMMO (spmoB). These interactions exhibit K_D values of 833 ± 409 nM and 9.0 ± 7.7 μM, respectively. The biochemical data combined with analysis of the crystal lattice interactions observed in the MDH structure suggest a model in which MDH and pMMO associate not as a discrete, stoichiometric complex but as a larger assembly scaffolded by the intracytoplasmic membranes.

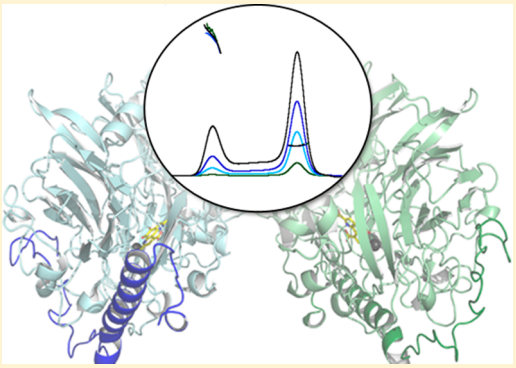

Methanotrophs are Gram-negative bacteria that utilize methane as their sole carbon and energy source.[1,2] As central players in the global carbon cycle and potential vehicles for new biological gas-to-liquid (GTL) conversion processes,[3] these organisms have been the focus of intense research efforts. The first step in their metabolic pathway is oxidation of methane by methane monooxygenases (MMOs).[4] The majority of methanotrophs utilize a membrane-bound or particulate MMO (pMMO)[5] that is located within extensive intracytoplasmic membranes. A few methanotroph strains can also express a soluble MMO (sMMO)[6] under conditions of copper starvation.[2,7] The product of the MMO reaction, methanol, is then converted to formaldehyde by methanol dehydrogenase (MDH) and either further oxidized to carbon dioxide via formaldehyde and formate dehydrogenases or assimilated into multicarbon compounds (Figure 1).[8,9]

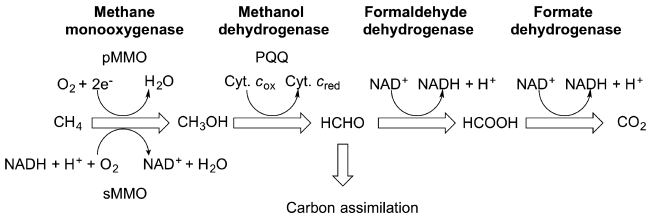

Figure 1. Metabolic pathway of *M. capsulatus* (Bath).

Most biochemical studies of methanotroph metabolism have addressed the most difficult step in the pathway, activation of the strong C−H bond in methane by MMOs. For pMMO, which is the predominant MMO in nature,[9] the major focus has been on determining the location and nature of the catalytic site. The pMMO from the well-studied methanotroph *Methylococcus capsulatus* (Bath) is an ∼300 kDa $\alpha_3\beta_3\gamma_3$ trimer,[10,11] comprising three copies each of the pmoB (α), pmoA (β), and pmoC (γ) subunits. The pmoA and pmoC subunits are composed primarily of transmembrane helices, and pmoB consists of two periplasmic cupredoxin-like domains linked by two transmembrane helices. The active site is proposed to be a dinuclear copper center located in the N-terminal pmoB periplasmic domain close to the membrane interface.[12,13] Another important, but less well studied, aspect of pMMO function is its relationship with the next enzyme in the pathway, MDH, which is located in the periplasm. MDHs are typically ∼145 kDa $\alpha_2\beta_2$ dimers containing a pyrroloquinoline quinone (PQQ)/calcium ion cofactor.[14,15] This cofactor is located in the α subunit (64 kDa); the exact function of the β subunit (8.5 kDa) remains unclear.[16]

Received: July 9, 2014
Revised: August 28, 2014
Published: September 3, 2014

dx.doi.org/10.1021/bi500850j | *Biochemistry* 2014, 53, 6211−6219

Several lines of evidence suggest that pMMO and MDH interact and could form a methane-to-formaldehyde oxidizing supercomplex. First, MDH has been localized not only to the periplasm but also to the intracytoplasmic membranes in *M. capsulatus* (Bath)[17] as well as in the methanotrophs *Methylomonas* sp. strain A4[18] and *Methylomicrobium album* BG8.[19] Second, Dalton and co-workers reported the isolation, purification, and structural characterization of a complex containing both pMMO and MDH.[20,21] This complex, which exhibited molecular masses of ~440−687 kDa depending on the technique used, was structurally characterized by cryoelectron microscopy (cryoEM) and single-particle analysis to 16 Å resolution. The resultant structure was interpreted as an $\alpha_3\beta_3\gamma_3$ trimer of pMMO capped on the periplasmic side by an $\alpha_3\beta_3$ trimer of MDH. In support of its functional relevance, the propylene epoxidation activity of this complex was moderately higher (2−5-fold)[20,21] than that of pMMO alone. However, the methane oxidation activity of this complex was not measured; only propylene epoxidation using duroquinol as a reductant and dye-linked oxidation of methanol were reported.

The potential existence of such a supercomplex *in vivo* is tantalizing because it would afford a direct route for methanol product from the pMMO periplasmic dicopper site to the methanol oxidation site in MDH. Moreover, a supercomplex might also provide insight into the physiological reductant of pMMO. Its electron donor is generally thought to be ubiquinol generated by a type 2 NADH:quinone oxidoreductase[22−24] but was proposed early on to be electrons recycled from the oxidation of methanol by MDH via the MDH electron acceptor, cytochrome c_L.[25,26] A pMMO−MDH complex, with the addition of cytochrome c_L,[27] could facilitate electron transfer without the requirement for NADH.[20,21]

Several aspects of the reported supercomplex have remained questionable, however. In all available MDH structures, a dimeric structure is observed,[15,28−33] and no biochemical evidence of the proposed trimeric state is available. In addition, the structure used in the cryoEM model is that of MDH from the methylotroph *Methylophilus methylotrophus* W3A1.[34,35] The structure of the cognate *M. capsulatus* (Bath) MDH has not been determined, hindering further consideration of the structural model. Moreover, the enhancement of pMMO propylene epoxidation activity by the presence of MDH could not be reconstituted by combining purified pMMO and MDH, and formation of a complex between purified pMMO and MDH has not been reported.[11,20] Thus, it remains unclear whether the interpretation of the observed supercomplex is accurate. To begin addressing these issues, we have isolated and purified native MDH from *M. capsulatus* (Bath), determined its oligomerization state and crystal structure, and investigated its interactions with *M. capsulatus* (Bath) pMMO using biolayer interferometry.

MATERIALS AND METHODS

Growth of *M. capsulatus* (Bath). *M. capsulatus* (Bath) was cultivated as described previously[36] using 12 L of sterile nitrate mineral salts medium supplemented with a solution of trace metals, 50 μM $CuSO_4$, and 80 μM $FeSO_4$. The pH of the medium was maintained at 6.8, with adjustments made using NaOH and H_2SO_4. Growth was initiated by the addition of ~10 g of frozen cell paste stock resuspended in sterile nitrate mineral salts medium at 45 °C. The fermentation was conducted at 45 °C with an air:methane gas ratio of 4:1 and an agitation rate of 300 rpm. Cells were harvested once the OD_{600} reached 5−7 and centrifuged for 10 min at 8000*g*. Pelleted cells were washed three times with 25 mM PIPES (pH 7.0), recentrifuged, flash-frozen in liquid nitrogen, and stored at −80 °C until they were ready for use.

Purification of MDH from *M. capsulatus* (Bath). *M. capsulatus* (Bath) cells (~20 g) were resuspended in lysis buffer [25 mM PIPES (pH 7.2) and 250 mM NaCl] and sonicated for 10 min (10 s on and 30 s off at 40% amplitude) on ice. The cell debris was removed by centrifugation at 24000*g* for 1 h, and membranes were separated from the soluble proteins by ultracentrifugation at 160000*g* for an additional 1 h. The membranes were then washed to isolate pMMO as described previously,[36] and the soluble fraction was used to purify MDH. The supernatant was dialyzed twice for 2 h into 20 mM Tris (pH 8.0) and then overnight to exchange the buffer.

The supernatant was loaded onto a DEAE-Sepharose FF XK 26/20 column (GE Healthcare) and washed with 20 mM Tris (pH 8.0) until all unbound protein eluted. MDH was eluted at ~50 mM NaCl using a gradient from 0 to 1 M NaCl in the same buffer. The fractions containing MDH were collected and concentrated using a Centriprep molecular weight cutoff (MWCO) 10 device. After concentration, MDH was loaded onto a HiLoad Superdex 75 16/600 prep grade column (GE Healthcare) pre-equilibrated with 20 mM Tris (pH 8.0) and 300 mM NaCl. MDH eluted in the void volume and was collected, and NH_4SO_4 powder was added slowly at 4 °C to a final concentration of 1.5 M. The sample was mixed at 4 °C for 1 h and then centrifuged at 12000*g* for 30 min at 4 °C. The resulting supernatant was loaded onto a HiTrap Butyl FF (GE Healthcare) column equilibrated with 50 mM Tris (pH 8.0), 150 mM NaCl, and 2 M NH_4SO_4 and eluted with a 0 to 10% glycerol gradient. Fractions containing MDH were pooled, concentrated with a Centriprep MWCO 30 device, and loaded onto a Superdex 200 16/600 column (GE Healthcare) equilibrated with 20 mM Tris (pH 8.0) and 300 mM NaCl. Initial protein masses were calculated from a calibration curve of protein standards analyzed on the Superdex 200 column, including ovalbumin (43 kDa), conalbumin (75 kDa), adolase (158 kDa), ferritin (440 kDa), and thyroglobin (669 kDa). The column void volume was determined with blue dextran to be 61 mL (elution time of 67 min). The protein concentration was determined using the Bradford assay with bovine serum albumin (BSA) as a standard. Enzyme activity was measured by the dichlorophenolindophenol (DCPIP) dye-linked dehydrogenase assay using phenazine methosulfate (PMS) as the mediator and methanol as the substrate.[37] The molar absorptivity of DCPIP at 600 nm is 1.91×10^7 M^{-1} cm^{-1}.

Deriphat-PAGE (D-PAGE) analysis[38,39] using 25 μg of purified *M. capsulatus* (Bath) pMMO and MDH was performed on a 4 to 16% Novex Bis-Tris gel (Novagen) using 12.5 mM Tris and 100 mM glycine (pH 8.3). The cathode buffer contained 0.2% (w/v) disodium *n*-lauryl-β-iminodipropionate (Deriphat) detergent. Gels were run at 100 V and 4 °C to improve the resolution and stained with Coomassie dye. In-gel activity assays were performed as described previously.[40,41] Briefly, the gel was incubated in a solution containing 50 mM Tris (pH 8.0), 15 mM NH_4Cl, 0.5 mM PMS, 1 mM nitroblue tetrazolium chloride (NBT), and 20 mM MeOH. Activity is detected by the reduction of NBT, which becomes blue in color. Once blue bands appeared, the reaction was stopped by the addition of water and the gel was compared with the Coomassie-stained gel.

Isolation, Solubilization, and Purification of pMMO from *M. capsulatus* (Bath). pMMO was purified as described previously with some modifications.[20] The membranes were isolated as described above, homogenized three times using a Dounce homogenizer, and resuspended in lysis buffer at a final concentration of 10−20 mg/mL, after which 1 mL aliquots were flash-frozen in liquid N_2 and stored at −80 °C. Frozen membranes were thawed on ice and washed three times with 25 mM PIPES (pH 7.2), 0.5 M NaCl, 1 mM benzamidine, and 40 μM $CuSO_4$. Washed membranes were then solubilized with the detergent *n*-dodecyl β-D-maltoside (DDM) (Anatrace) by the addition of 1.5 mg of DDM/mg of protein at 4 °C for at least 1 h while being gently stirred. The sample was concentrated to 20 mg/mL using a Centriprep MWCO 50 device and loaded onto a Superdex 200 16/600 column (GE Healthcare) pre-equilibrated with 25 mM PIPES (pH 7.2), 150 mM NaCl, 0.03% DDM, and 1 mM benzamidine. Sample purity was assessed by sodium dodecyl sulfate−polyacrylamide gel electrophoresis (SDS−PAGE), and pure fractions were collected and concentrated with a Centriprep MWCO 50 device to 10−20 mg/mL. Samples were flash-frozen and stored at −80 °C. The protein concentration was determined by the Detergent-Compatible Lowry Assay (Bio-Rad) using BSA as a standard. The recombinant spmoB protein, which corresponds to the soluble domains of the pMMO pmoB subunit, was prepared as described previously.[12,42]

Size Exclusion Chromatography with Multi-angle Light Scattering (SEC-MALS). The molecular mass of MDH at various protein concentrations was determined by conducting SEC-MALS experiments. Analyses were performed using an Agilent Technologies 1100 LC high-performance liquid chromatography system (Agilent Technologies, Santa Clara, CA) equipped with a Dawn Heleos II 18-angle MALS light scattering detector, an Optilab T-rEX (refractometer with extended range) refractive index detector, a WyattQELS quasi-elastic (dynamic) light scattering (QELS) detector, and ASTRA software for data analysis (all from Wyatt Technology, Santa Barbara, CA). Varying concentrations of MDH in 25 mM PIPES (pH 7.25), 1 mM benzamidine, and 0.03% DDM (100 μL sample size) were injected onto a pre-equilibrated Superdex 200 10/300 GL column (GE Healthcare) at a flow rate of 0.5 mL/min at room temperature. The ASTRA software was used to calculate the molecular mass of the $\alpha_2\beta_2$ dimer and higher-order oligomers. This software also determines the polydispersity of the protein sample across the elution peaks. The buffer differential index of refraction, d*n*/d*c*, was determined to be 0.18 mL/g, and BSA was used as a control protein. The relative percentages of the dimer and multimer were determined from the UV−vis elution profiles using Chemstation software (Agilent).

Biolayer Interferometry. The affinity of purified MDH for purified pMMO, both from *M. capsulatus* (Bath), was determined using a ForteBio BLItz biolayer interferometer in the Northwestern Keck Biophysics Facility. Amine reactive second-generation (AR2G) biosensors (ForteBio) were hydrated in 15 mM NaOAc (pH 5.5) for 10 min prior to each experimental run. A single run is divided into six steps: (i) buffer baseline, in which the amine reactive sensor is immersed in 15 mM NaOAc (pH 5.5) for 60 s to establish a zero baseline; (ii) sensor activation, in which biosensors are activated for 5 min with a mixture of 20 mg/mL EDC {1-ethyl-3-[3-(dimethylamino)propyl]carbodiimide hydrochloride} and 5 mg/mL sulfo-NHS (*N*-hydroxysulfosuccinimide) in water; (iii) ligand loading, in which MDH diluted to 1 mg/mL with 15 mM NaOAc (pH 5.5) is reacted with the biosensor for 5 min and then deactivated for 5 min with 1 M ethanolamine (pH 8.5); (iv) baseline, in which the biosensor is immersed in either pMMO buffer [25 mM PIPES (pH 7.2), 1 mM benzamidine, and 0.03% DDM] or spmoB buffer [50 mM Tris (pH 8.0) and 150 mM NaCl] for 2 min to remove any unbound MDH; (v) association, in which the amine-reacted MDH biosensor tip is immersed in purified pMMO or refolded spmoB for 5 min; and (vi) dissociation, in which the MDH−protein complex formed during association is transferred to the corresponding buffer for 5 min to dissociate. Runs were performed with pMMO concentrations of 0.5−5 μM. Sample runs with spmoB were performed at protein concentrations of 0.3−30 μM. Immobilized BSA was used as a negative control at a concentration of 0.3 mg/mL with 30 μM spmoB. A new biosensor tip was used for each run. The sensorgrams were corrected against a buffer only reference and fit with the ForteBio Data Analysis package assuming a 1:1 Langmuir binding model with the global fitting function.

Determination of the Structure of MDH from *M. capsulatus* (Bath). For crystallization, MDH was exchanged into 25 mM HEPES (pH 7.5), 150 mM NaCl, and 10% glycerol and concentrated to 20 mg/mL. Crystals were obtained by the hanging drop diffusion method at 4 °C by mixing 2 μL of protein with 1 μL of a reservoir solution containing 0.1 M NaHEPES (pH 7.5) and 30% PEG 4000. Rhombic crystals formed overnight. The crystals were cryoprotected in a reservoir solution containing 40% 2-methyl-2,4-pentanediol (MPD) and flash-frozen in liquid N_2. Data were collected at sector 21 (Life Sciences Collaborative Access Team, LS-CAT) of the Advanced Photon Source at Argonne National Laboratory. Initial data processing and integration were conducted using HKL2000,[43] with the resolution limits determined by inspection. After the initial model was built, the data were reprocessed using the xia2[44] pipeline to XDS[45] and scaled with AIMLESS.[46] This reprocessing was conducted to ensure that the high R_{merge} values from HKL2000 are not due to an inappropriate resolution limit. The resolution is determined automatically by xia2, and both programs gave a resolution cutoff of 2.57 Å. The data collection statistics are summarized in Table 1.

The structure of MDH was determined by molecular replacement with Phaser[47] from the CCP4 program suite,[48] using the coordinates of *Me. methylotrophus* W3A1 MDH (Protein Data Bank entry 2AD7) as a starting model.[49] Initial refinement was conducted with Refmac,[50] followed by several rounds of refinement with phenix.refine,[51] which fixes rotamer geometry and water coordination and manually flips His/Asn/Gln residues. COOT was used for manual building of the structure and structural alignments.[52] Coordinates for the ligand pyrroloquinoline quinone (PQQ) were obtained from the *Me. methylotrophus* W3A1 MDH structure, and the library of restraints was generated using the eLBOW[51] program available in Phenix. The final structure was validated by Molprobity[53] and the Phenix validation software (Table 1). Protein−protein interface analysis was conducted using the PISA server at the European Bioinformatics Institute (http://www.ebi.ac.uk/pdbe/prot_int/pistart.html).[54]

RESULTS

Isolation and Purification of MDH from *M. capsulatus* (Bath). Purification of MDH from *M. capsulatus* (Bath) has

Table 1. *M. capsulatus* (Bath) MDH Data Collection and Refinement Statistics

Data Collection[a]	
space group	$P2_12_12_1$
unit cell	
a, *b*, *c* (Å)	128.49, 210.29, 231.42
wavelength (Å)	0.97856
resolution (Å)	105.15−2.57 (2.64−2.57)
R_{merge}[b]	0.193 (0.815)
mean $I/\sigma(I)$	10.5 (2.6)
completeness (%)	100 (100)
multiplicity	7.6 (7.7)
no. of unique reflections	199109 (14539)
$CC_{1/2}$ (%)	99.0 (81.3)
Refinement	
R_{work}/R_{free}	0.1575/0.2081
average *B* factor (Å^2)	25.0
no. of atoms	43059
ligand	192
solvent	2404
rmsd	
bond lengths (Å)	0.005
bond angles (deg)	0.933
Ramachandran plot (%)	
favored	94.8
outliers	0.4
rotamer outliers	0.5
Molprobity Clashscore	4.1

[a]Values in parentheses are for the highest-resolution shell. [b]$R_{merge} = \sum_{hkl}\sum_i|I_i(hkl) - \langle I(hkl)\rangle|/\sum_{hkl}\sum_i I_i(hkl)$.

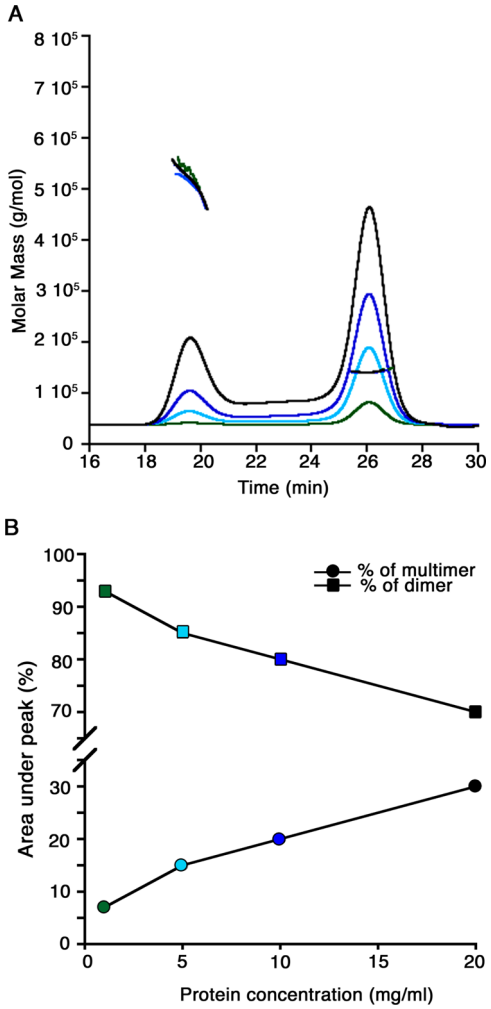

Figure 2. Oligomerization states of *M. capsulatus* (Bath) MDH in solution. (A) SEC-MALS analysis of MDH at varying protein concentrations. The signals from the refractive index detector are shown as a function of elution time (black for 20 mg/mL, blue for 10 mg/mL, cyan for 5 mg/mL, and green for 1 mg/mL). The thick horizontal lines indicate the calculated molecular masses of the eluting peaks. (B) Comparison of the multimer and dimer peak areas (as percentages) from the SEC-MALS experiments displayed as a line graph. An increased protein concentration results in an increase in multimer percentage concomitant with a decrease in dimer percentage. The colors of the data points correspond to the SEC-MALS traces in panel A.

been reported previously.[55,56] For this study, MDH was isolated from the *M. capsulatus* (Bath) soluble supernatant during membrane isolation. MDH is present at high levels in the soluble fraction and could be monitored during purification by following the PQQ cofactor absorbance at 345 nm. After four column chromatography steps, a >90% pure sample of MDH was obtained (Figure S1 of the Supporting Information) with a typical yield of ∼30 mg/L. The purified MDH exhibits a specific activity of 183 ± 32 nmol min^{-1} mg^{-1} as measured by the dye-linked DCPIP assay, in close agreement with previously reported values for *M. capsulatus* (Bath) MDH.[55,56]

Solution Oligomerization State of *M. capsulatus* (Bath) MDH. Initial size exclusion chromatography (SEC) analysis shows a single peak with a molecular mass of ∼144 kDa, corresponding to the $\alpha_2\beta_2$ dimer. After the sample is concentrated, stored at −80 °C, and then thawed, a second peak attributable to a higher-order oligomer appears (Figure S2 of the Supporting Information). These results are consistent with the previous observation of two distinct oligomeric species by single-particle analysis of electron micrographs.[55] The MDH oligomerization state was further investigated by SEC coupled to an in-line multi-angle light scattering detector (SEC-MALS). This technique determines the molecular mass of a protein independent of its SEC elution profile.[57] Four MDH samples with concentrations of up to 20 mg/mL were analyzed by SEC-MALS. All samples eluted as two peaks, the first (19.5 mL) corresponding to a molecular mass of ∼460−560 kDa and the second (26 mL) to a molecular mass of 144 kDa, which is the $\alpha_2\beta_2$ dimer (Figure 2A). The higher-mass species is much less homogeneous than the dimer as indicated by the distribution of masses detected by light scattering (Figure 2A). Its mass suggests the presence of three or four $\alpha_2\beta_2$ dimers, assuming a mass of ∼72.5 kDa (http://expasy.org) for the $\alpha\beta$ monomer.

The fraction of MDH present as the oligomer increases with increasing protein concentrations (Figure 2). At 1 mg/mL, the protein exists as ∼90% dimer and 10% oligomer, whereas at 20 mg/mL, the percentages shift to 70% dimer and 30% oligomer (Figure 2B). Because of saturation of the MALS detector, concentrations of >20 mg/mL could not be analyzed by this technique, but analysis of MDH concentrated to >100 mg/mL using the same column matrix coupled to a UV−vis detector (Figure S3 of the Supporting Information) indicates the presence of 10% dimer and 90% oligomer. Reanalysis of either the dimer or oligomer fraction on the same column indicates the presence of both species. Thus, the dimer and the oligomer are in equilibrium, and the oligomer begins to associate more

dx.doi.org/10.1021/bi500850j | *Biochemistry* 2014, 53, 6211−6219

readily at high concentrations (Figure S3 of the Supporting Information).

The dimer and higher-order oligomers are also evident on native D-PAGE gels stained with Coomassie and treated with PMS and NBT to detect MDH activity (Figure 3). Both the

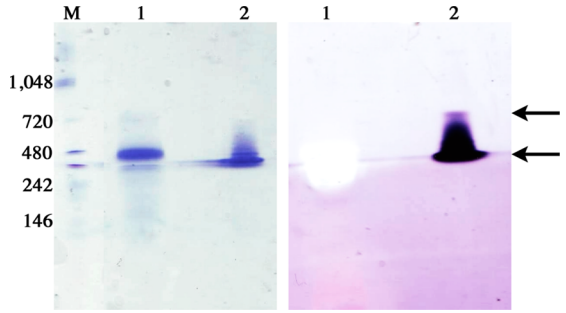

Figure 3. D-PAGE analysis of pMMO and MDH from *M. capsulatus* (Bath). Gels were either stained with Coomassie dye (left) or reacted with PMS, NBT, and methanol to detect MDH activity (right). Equal amounts (25 μg) of pMMO (lane 1) and MDH (lane 2) were loaded per gel. Molecular mass markers are shown in lane M (kDa). The arrows indicate the putative MDH dimer and oligomer species.

dimer and the oligomer exhibit MDH activity, whereas no activity is detected for pMMO, which was used as a control. The major species observed by D-PAGE is the dimer, consistent with the low protein concentration used for the gel. This result indicates that the oligomeric MDH species observed by SEC and SEC-MALS represent an active form of MDH.

Interaction between MDH and pMMO from *M. capsulatus* (Bath). The possibility of a specific protein−protein interaction between MDH and pMMO was investigated by biolayer interferometry. MDH was immobilized on an amine chip using standard NHS/EDC coupling at 1 mg/mL, and interactions with pMMO (0.5−5 μM) were assayed. A concentration-dependent interaction between immobilized MDH and pMMO was observed (Figure 4A). Analysis of the sensorgram data yielded a K_D value of 833 ± 409 nM. To assess whether the interaction could be related to the proposed complex between MDH and the periplasmic domains of pMMO, we also conducted experiments with spmoB (0.3−30 μM). A weaker interaction was observed, yielding a K_D value of 9.0 ± 7.7 μM (Figure 4B). Control experiments performed with BSA showed no interaction (Figure 4C). Attempts to isolate a MDH−pMMO complex by SEC were not successful, however.

Overall Structure of *M. capsulatus* (Bath) MDH. The *M. capsulatus* (Bath) MDH X-ray structure was determined to 2.57 Å resolution. MDH crystallizes with four $\alpha_2\beta_2$ protomers in the asymmetric unit (chains A/J and E/M, chains B/I and G/O, chains C/K and D/L, and chains F/N and H/P). The average rmsd between protomers is 0.189 Å, using chain A (α subunit) and chain J (β subunit) as the reference protomer. Because of the presence of periplasmic signal sequences, the model for the α subunit begins at Asn 29, and the model for the β subunit begins at Tyr 23. There are no gaps within the chains. The β subunit in protomers I−L is modeled through Ile 93, whereas the C-terminal residue, Lys 94, is also modeled in protomers M−P.

The overall fold is the same as those of other MDH structures, with eight antiparallel four-stranded β sheets

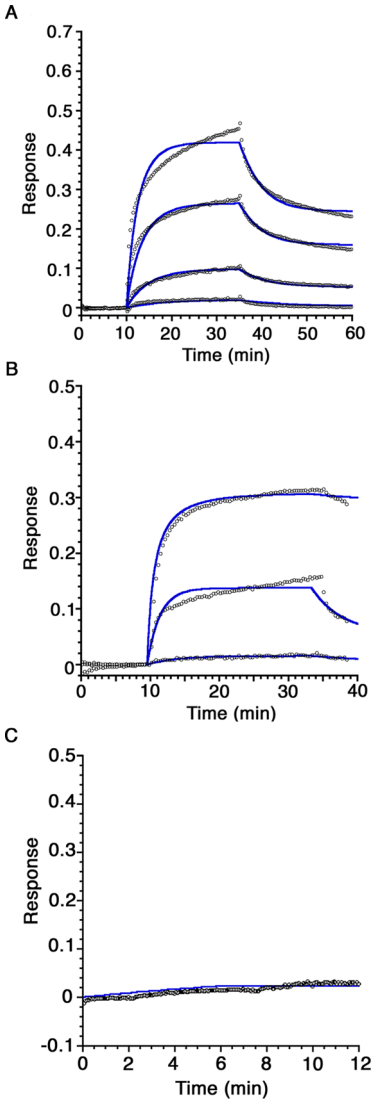

Figure 4. Biolayer interferometry sensorgrams of the protein−protein interactions of immobilized *M. capsulatus* (Bath) MDH. (A) Purified *M. capsulatus* (Bath) pMMO samples at concentrations of 0.5, 1, 2.5, and 5 μM were monitored for binding to immobilized MDH. The data fitting curves are displayed as blue lines. (B) Refolded spmoB samples at concentrations of 0.3, 3, and 30 μM were reacted with immobilized MDH. (C) Immobilized BSA was monitored for interaction with 30 μM spmoB. No binding response is observed. Each experiment was repeated with three independent biological samples.

forming a propeller.[15] Each four-stranded β sheet blade in the propeller has the typical "W" motif, and the blades are labeled W1−W8 according to nomenclature from previous structures (Figure 5A).[28] There are several flanking α helices as well as an additional β hairpin and a three-stranded sheet insertion between propeller blades W5 and W6 (Figure 5A). The PQQ cofactor and Ca^{2+} ion are located in the center of the propeller as in other MDH structures. The PQQ is sandwiched between Trp 271 and a disulfide bond formed by residues Cys 131 and Cys 132 common to other methanol dehydrogenase enzymes.[14,15] An extensive hydrogen bonding network stabilizes the PQQ. The Ca^{2+} ion is coordinated by the PQQ C-7 carboxylate, C-5 carbonyl, and N-6 quinoline nitrogen moieties as well as residues Glu 205, Asn 289, and Asp 331 (Figure 5B).

dx.doi.org/10.1021/bi500850j | *Biochemistry* 2014, 53, 6211−6219

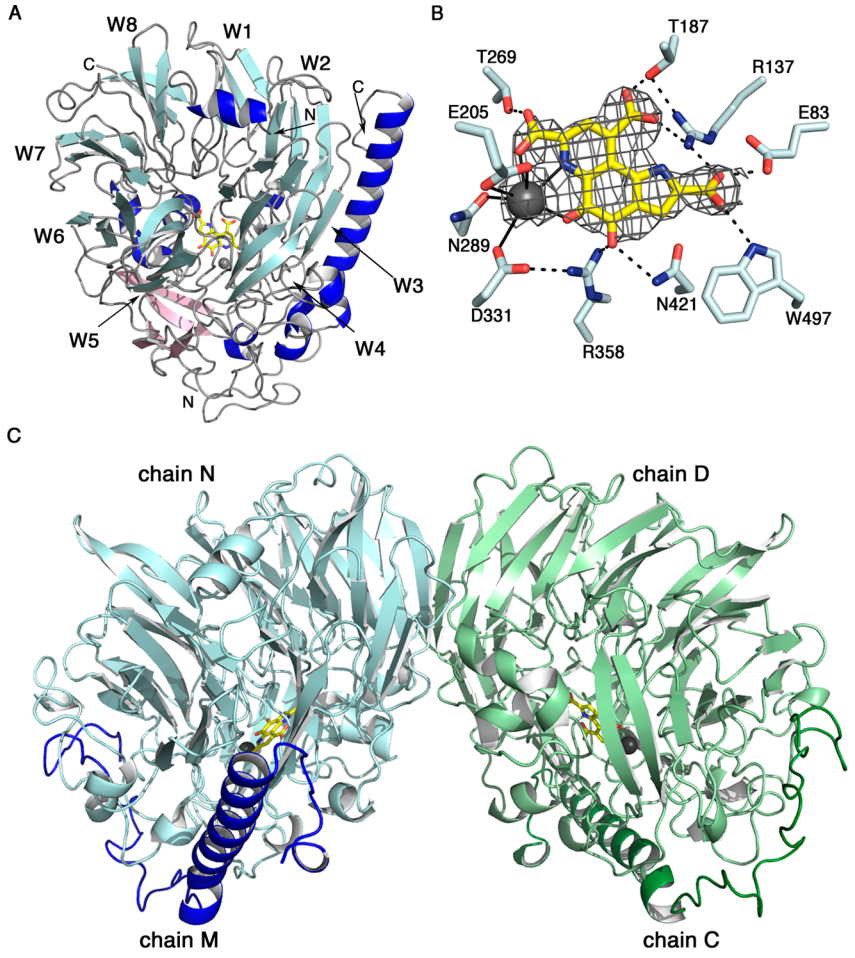

Figure 5. Structure of *M. capsulatus* (Bath) MDH. (A) $\alpha\beta$ protomer. The eight-bladed β sheet propeller motif is colored light blue, and the blades are labeled W1−W8. Auxiliary β strands are colored light pink and α helices blue, including the long α helix of the β subunit. A PQQ ligand (yellow) and Ca^{2+} ion (gray) are located in the cavity of the propeller core fold. (B) Composite omit map generated in Phenix contoured at 1σ showing the cofactors and hydrogen bonding residues. Ligand coordination to the Ca^{2+} ion is shown as solid lines, and hydrogen bonds are shown as dashed lines. (C) $\alpha_2\beta_2$ dimer structure with chains C and D colored light and dark green and chains M and N colored light and dark blue.

The β subunit is mainly α helical in structure and extends the length of the α subunit between β sheets W2 and W3 of the propeller motif (Figure 5A). The N-terminus of the β subunit contains a flexible loop region from residue Tyr 23 to Asp 55 before the long α helix begins at residue Pro 56. Each β subunit interacts extensively with its associated α subunit. These interactions include three salt bridges. Residue Lys 38 from the β subunit interacts with Glu 295 and Glu 329 from the α subunit; residue Glu 70 from the β subunit interacts with Arg 225 from the α subunit, and residues Arg 72 and Arg 76 from the β subunit interact with Glu 176 from the α subunit.

Secondary structure matching with COOT between the structures of the $\alpha\beta$ protomers of *M. capsulatus* (Bath) MDH (644 residues) and *Me. methylotrophus* W3A1 MDH (640 residues)[49] results in a sequence identity of 65%. This superposition of 631 residues yields an rmsd of 0.69 Å and reveals several minor gaps and insertions in loop regions as well as some substitutions at the PQQ binding site. Residues Met 102 and Ser 162 in *Me. methylotrophus* W3A1 MDH both hydrogen bond to PQQ and are replaced with alanines in the *M. capsulatus* (Bath) MDH structure. In addition, Cys 144 and Cys 167 (*Me. methylotrophus* W3A1 numbering) are both serine residues in *M. capsulatus* (Bath) MDH, resulting in one fewer intrachain disulfide bond, though this substitution is common in other MDHs.

Oligomerization State of *M. capsulatus* (Bath) MDH in the Crystal Structure. The dimer detected by SEC-MALS is observed in the structure and corresponds to the previously observed $\alpha_2\beta_2$ dimer (Figure 5C). The surface area of the dimer interface is ∼1400 Å^2. The dimer is saddle-shaped with the two β subunits, which are not involved in dimerization, located in the stirrups position of the saddle. In the dimer, the two α subunits interact via β strands from propeller blades W7 and W8, forming an extended β sheet network. There are additional interactions between the C-terminal loop regions of each chain and the loop region after propeller blade W1. The interface includes approximately 30 hydrogen bonds. Among key interacting residues are Arg 112 and Gln 532, which correspond to Gly 84 and Lys 502, respectively, in *Me. methylotrophus* W3A1 MDH.[49] Further comparison of the interfaces reveals 22 hydrogen bonds at the *Me. methylotrophus* W3A1 MDH dimer interface as compared to 30 in *M. capsulatus* (Bath) MDH.

Within the crystal lattice, the dimers pack together in alternating pairs with all the lattice contacts involving the α subunits. The net result is a bilayer-like structure with the β subunits on opposite sides pointing toward the solvent channels (Figure 6). Interface analysis with PDBePISA[54]

dx.doi.org/10.1021/bi500850j | *Biochemistry* 2014, 53, 6211−6219

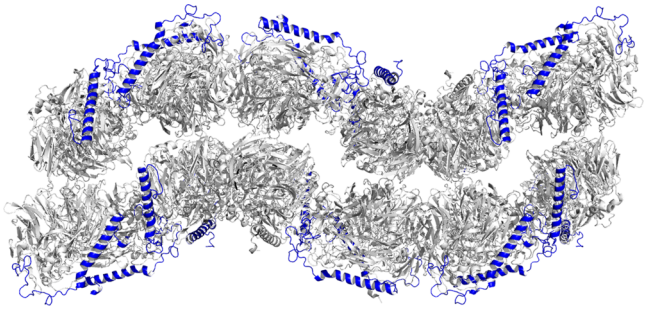

Figure 6. Crystal packing interactions of MDH from *M. capsulatus* (Bath). Symmetry-related molecules of MDH reveal a bilayer-like packing arrangement with the β subunit exposed to the solvent. The α subunit is colored gray and the β subunit blue.

indicates that no higher-order stable oligomers are present. Thus, the ∼460−560 kDa species detected by SEC-MALS is likely not represented by the arrangement of molecules in the crystal structure. This is not surprising because the $\alpha_2\beta_2$ dimer fraction was isolated by SEC (Figure S2 of the Supporting Information), and the dimer is predominant at the concentration of 20 mg/mL used for crystallization.

DISCUSSION

These data indicate that *M. capsulatus* (Bath) MDH is primarily an $\alpha_2\beta_2$ dimer in solution but can form ∼460−560 kDa oligomers at high concentrations, which also exhibit MDH activity (Figure 3). The oligomeric species is heterogeneous, and there is no evidence of the existence in solution of an $\alpha_3\beta_3$ trimer, as proposed for the complex characterized by cryoEM.[21] In addition, an interaction between MDH and pMMO has been detected by biolayer interferometry. This interaction appears to be specific as demonstrated by control experiments with spmoB and BSA. Finally, the *M. capsulatus* (Bath) MDH crystal structure reveals a dimer that is similar to other MDH structures. No unusual higher-order oligomers are present in the structure.

Taken together, these findings have several important implications for the proposed pMMO−MDH supercomplex. First, the biolayer interferometry data provide evidence of direct interactions between the two isolated enzymes. Because the α and β subunits of MDH contain a large number of exposed lysine residues, the immobilization is nonspecific, preventing identification of the MDH regions involved in interaction with pMMO. The fact that an interaction is also detected with spmoB, which includes only the periplasmic domains of pMMO, is consistent with MDH's location in the periplasm as well as with numerous studies indicating that MDH can be associated with the membranes.[17−19] It is not surprising that the interaction of MDH with pMMO is an order of magnitude stronger than that with spmoB because spmoB alone does not form trimers and has limited solubility.[12] Despite the biolayer interferometry data, we were not able to isolate a stable pMMO−MDH complex by SEC, consistent with previous studies in which the complex and its activity could not be reconstituted by combining purified proteins.[11,20] Thus, the association may be dynamic and likely depends on the presence of the membrane or additional protein components. Affixing MDH to the biosensor surface may partially mimic such requirements.

The observed oligomerization states of MDH in solution and in the crystal also suggest that interactions both among MDH dimers and between MDH and pMMO are transient and/or facilitated by additional components. The cryoEM model was suggested to represent an $\alpha_3\beta_3$ trimer of MDH capping the periplasmic regions of the pMMO trimer.[21] One $\alpha_2\beta_2$ dimer was fit into two lobes of density, but it was not clear whether an $\alpha\beta$ protomer from a second dimer could fit the third lobe or whether a new trimeric $\alpha_3\beta_3$ structure would be required. The SEC-MALS data indicate that ∼460−560 kDa *M. capsulatus* (Bath) MDH oligomers can form at high concentrations; such a mass would be consistent with three or four $\alpha_2\beta_2$ dimers or two or three $\alpha_3\beta_3$ trimers. However, the *M. capsulatus* (Bath) MDH structure reveals an $\alpha_2\beta_2$ dimer similar to other MDH structures with no evidence of a stable higher-order oligomerization state. Given the absence of a stable assembly in the ∼460−560 kDa range in the structure and the heterogeneity detected by SEC-MALS, it seems unlikely that a discrete higher-order oligomerization state interacts with pMMO. Instead, a more transient association of MDH dimers may occur in the presence of membrane-embedded pMMO.

The crystal packing arrangement provides some insight into how multiple MDH dimers might assemble *in vivo*. In the crystal, the dimers are arranged in pairs. The ∼460−560 kDa species observed by SEC-MALS may represent a partial assembly of MDH dimers into weakly associated pairs. Within the crystal lattice, all the β subunits are exposed to the solvent (Figure 6). The β subunit is lysine-rich (11 of 72 residues), with five lysines at the N-terminus and the remainder protruding from the C-terminal α helix. The exact function of the β subunit and these lysine residues is not known. One possibility suggested previously for methylotrophs is docking with cytochrome c_L via electrostatic interactions,[58] although cross-linking data point to interactions with the α subunit.[59,60] Alternatively, the positively charged lysine residues might interact with pMMO or with negatively charged phospholipid headgroups at the periplasmic membrane surface, analogous to the lysine-mediated binding of the yeast copper chaperone for superoxide dismutase (CCS) to lipid bilayers. In that system, interaction with the membrane allows CCS to find its source of copper, the transporter Ctr1.[61]

Importantly, the intracytoplasmic membranes in methanotrophs typically form stacked or bundled structures.[1,2,18,19] It is possible to envision a "bilayer" of MDH as observed in the crystal lattice (Figure 6) interacting with multiple sections of the pMMO-containing membranes. The formation of intracytoplasmic membranes accompanies pMMO expression,[62,63] and beyond housing pMMO, these membranes likely play a role in assembling other membrane-bound and periplasmic proteins, including respiratory complexes. Further study of the interplay among pMMO, MDH, intracytoplasmic membranes, and other metabolic enzymes is an important direction for future work.

ASSOCIATED CONTENT

Supporting Information

SDS−PAGE analysis of purified *M. capsulatus* (Bath) MDH and SEC analysis of purified *M. capsulatus* (Bath) MDH. This material is available free of charge via the Internet at http://pubs.acs.org.

Accession Codes

The coordinates and structure factors have been deposited as Protein Data Bank entry 4TQO.

AUTHOR INFORMATION

Corresponding Author

*E-mail: amyr@northwestern.edu. Telephone: (847) 467-5301.

Funding

This work was supported by National Institutes of Health Grants GM070473 (A.C.R.) and F32GM097049 (M.A.C.).

Notes

The authors declare no competing financial interest.

ACKNOWLEDGMENTS

We thank Corey Janczak of the Northwestern Keck Biophysics Facility for assistance with instrumentation, data collection, and data interpretation. In addition, we thank Sarah Sirajuddin for assistance with *M. capsulatus* (Bath) fermentation, Eliza Zielazinski for assistance with initial purification steps, and Thomas Lawton for assistance with D-PAGE. Use of the Advanced Photon Source, an Office of Science User Facility operated for the U.S. Department of Energy (DOE) Office of Science by Argonne National Laboratory, was supported by the U.S. DOE under Contract DE-AC02-06CH11357. Use of LS-CAT Sector 21 was supported by the Michigan Economic Development Corp. and the Michigan Technology Tri-Corridor (Grant 085P1000817).

ABBREVIATIONS

MMO, methane monooxygenase; sMMO, soluble methane monooxygenase; pMMO, particulate methane monooxygenase; MDH, methanol dehydrogenase; PQQ, pyrroloquinoline quinone; cryoEM, cryoelectron microscopy; SEC-MALS, size exclusion chromatography with multi-angle light scattering; PMS, phenazine methosulfate; NBT, nitroblue tetrazolium; rmsd, root-mean-square deviation; D-PAGE, Deriphat-polyacrylamide gel electrophoresis.

REFERENCES

(1) Hanson, R. S., and Hanson, T. E. (1996) Methanotrophic bacteria. *Microbiol. Rev. 60*, 439−471.

(2) Semrau, J. D., Dispirito, A. A., and Yoon, S. (2010) Methanotrophs and copper. *FEMS Microbiol. Lett. 34*, 496−531.

(3) Fei, Q., Guarnieri, M. T., Tao, L., Laurens, L. M., Dowe, N., and Pienkos, P. T. (2014) Bioconversion of natural gas to liquid fuel: Opportunities and challenges. *Biotechnol. Adv. 32*, 596−614.

(4) Hakemian, A. S., and Rosenzweig, A. C. (2007) The biochemistry of methane oxidation. *Annu. Rev. Biochem. 76*, 223−241.

(5) Culpepper, M. A., and Rosenzweig, A. C. (2012) Architecture and active site of particulate methane monooxygenase. *Crit. Rev. Biochem. Mol. Biol. 47*, 483−492.

(6) Tinberg, C. E., and Lippard, S. J. (2011) Dioxygen activation in soluble methane monooxygenase. *Acc. Chem. Res. 44*, 280−288.

(7) Murrell, J. C., McDonald, I. R., and Gilbert, B. (2000) Regulation of expression of methane monooxygenases by copper ions. *Trends Microbiol. 8*, 221−225.

(8) Trotsenko, Y. A., and Murrell, J. C. (2008) Metabolic aspects of aerobic obligate methanotrophy. In *Advances in Applied Microbiology* (Laskin, A. L., and Sariaslani, S., Eds.) Vol. *63*, pp 183−229, Elsevier Academic Press Inc., San Diego.

(9) Chistoserdova, L., and Lidstrom, M. E. (2013) Aerobic methylotrophic prokaryotes. In *The Prokaryotes: Prokaryotic physiology and biochemistry* (Rosenberg, E., DeLong, E. F., Thompson, F., Lory, S., and Stackebrandt, E., Eds.) 4th ed., pp 267−285, Springer-Verlag, Berlin.

(10) Lieberman, R. L., and Rosenzweig, A. C. (2005) Crystal structure of a membrane-bound metalloenzyme that catalyses the biological oxidation of methane. *Nature 434*, 177−182.

(11) Kitmitto, A., Myronova, N., Basu, P., and Dalton, H. (2005) Characterization and structural analysis of an active particulate methane monooxygenase trimer from *Methylococcus capsulatus* (Bath). *Biochemistry 44*, 10954−10965.

(12) Balasubramanian, R., Smith, S. M., Rawat, S., Stemmler, T. L., and Rosenzweig, A. C. (2010) Oxidation of methane by a biological dicopper centre. *Nature 465*, 115−119.

(13) Culpepper, M. A., Cutsail, G. E., Hoffman, B. M., and Rosenzweig, A. C. (2012) Evidence for oxygen binding at the active site of particulate methane monooxygenase. *J. Am. Chem. Soc. 134*, 7640−7643.

(14) Anthony, C. (2004) The quinoprotein dehydrogenases for methanol and glucose. *Arch. Biochem. Biophys. 428*, 2−9.

(15) Anthony, C., and Williams, P. (2003) The structure and mechanism of methanol dehydrogenase. *Biochim. Biophys. Acta 1647*, 18−23.

(16) Gvozdev, A. R., Tukhvatullin, I. A., and Gvozdev, R. I. (2012) Quinone-dependent alcohol dehydrogenases and FAD-dependent alcohol oxidases. *Biochemistry (Moscow) 77*, 843−856.

(17) Wadzinski, A. M., and Ribbons, D. W. (1975) Oxidation of C1 compounds by particulate fractions from *Methylococcus capsulatus*: Properties of methanol oxidase and methanol dehydrogenase. *J. Bacteriol. 122*, 1364−1374.

(18) Fassel, T. A., Buchholz, L. A., Collins, M. L. P., and Remsen, C. C. (1992) Localization of methanol dehydrogenase in two strains of methylotrophic bacteria detected by immunogold labeling. *Appl. Environ. Microbiol. 58*, 2302−2307.

(19) Brantner, C. A., Remsen, C. C., Owen, H. A., Buchholz, L. A., and Collins, M. L. P. (2002) Intracellular localization of the particulate methane monooxygenase and methanol dehydrogenase in *Methylomicrobium album* BG8. *Arch. Microbiol. 178*, 59−64.

(20) Basu, P., Katterle, B., Andersson, K. K., and Dalton, H. (2003) The membrane-associated form of methane monooxygenase from *Methylococcus capsulatus* (Bath) is a copper/iron protein. *Biochem. J. 369*, 417−427.

(21) Myronova, N., Kitmitto, A., Collins, R. F., Miyaji, A., and Dalton, H. (2006) Three-dimensional structure determination of a protein supercomplex that oxidizes methane to formaldehyde in *Methylococcus capsulatus* (Bath). *Biochemistry 45*, 11905−11914.

(22) Cook, S. A., and Shiemke, A. K. (2002) Evidence that a type-2 NADH:quinone oxidoreductase mediates electron transfer to particulate methane monooxygenase in *Methylococcus capsulatus*. *Arch. Biochem. Biophys. 398*, 32−40.

(23) Choi, D. W., Kunz, R. C., Boyd, E. S., Semrau, J. D., Antholine, W. E., Han, J. I., Zahn, J. A., Boyd, J. M., de la Mora, A. M., and DiSpirito, A. A. (2003) The membrane-associated methane monooxygenase pMMO and pMMO-NADH:quinone oxidoreductase complex from *Methylococcus capsulatus* Bath. *J. Bacteriol. 185*, 5755−5764.

(24) Shiemke, A. K., Arp, D. J., and Sayavedra-Soto, L. A. (2004) Inhibition of membrane-bound methane monooxygenase and ammonia monooxygenase by diphenyliodonium: Implications for electron transfer. *J. Bacteriol. 186*, 928−937.

(25) Tonge, G. M., Harrison, D. E. F., Knowles, C. J., and Higgins, I. J. (1975) Properties and partial purification of the methane-oxidizing enzyme system from *Methylosinus trichosporium*. *FEBS Lett. 58*, 293−299.

(26) Leak, D. J., and Dalton, H. (1986) Growth yields of methanotrophs. 2. A theoretical analysis. *Appl. Microbiol. Biotechnol. 23*, 477−481.

(27) Anthony, C. (1992) The *c*-type cytochromes of methylotrophic bacteria. *Biochim. Biophys. Acta 1099*, 1−15.

(28) Ghosh, M., Anthony, C., Harlos, K., Goodwin, M. G., and Blake, C. (1995) The refined structure of the quinoprotein methanol dehydrogenase from *Methylobacterium extorquens* at 1.94 Å. *Structure 3*, 177−187.

(29) Xia, Z. X., Dai, W. W., Zhang, Y. F., White, S. A., Boyd, G. D., and Mathews, F. S. (1996) Determination of the gene sequence and

the three-dimensional structure at 2.4 Å resolution of methanol dehydrogenase from *Methylophilus* W3A1. *J. Mol. Biol. 259*, 480−501.
(30) Xia, Z. X., Dai, W. W., He, Y. N., White, S. A., Mathews, F. S., and Davidson, V. L. (2003) X-ray structure of methanol dehydrogenase from *Paracoccus denitrificans* and molecular modeling of its interactions with cytochrome *c*-551i. *JBIC, J. Biol. Inorg. Chem. 8*, 843−854.
(31) Williams, P. A., Coates, L., Mohammed, F., Gill, R., Erskine, P. T., Coker, A., Wood, S. P., Anthony, C., and Cooper, J. B. (2005) The atomic resolution structure of methanol dehydrogenase from *Methylobacterium extorquens*. *Acta Crystallogr. D61*, 75−79.
(32) Nojiri, M., Hira, D., Yamaguchi, K., Okajima, T., Tanizawa, K., and Suzuki, S. (2006) Crystal structures of cytochrome c_L and methanol dehydrogenase from *Hyphomicrobium denitrificans*: Structural and mechanistic insights into interactions between the two proteins. *Biochemistry 45*, 3481−3492.
(33) Pol, A., Barends, T. R. M., Dietl, A., Khadem, A. F., Eygensteyn, J., Jetten, M. S. M., and Op den Camp, H. J. M. (2014) Rare earth metals are essential for methanotrophic life in volcanic mudpots. *Environ. Microbiol. 16*, 255−264.
(34) Xia, Z. X., He, Y. N., Dai, W. W., White, S. A., Boyd, G. D., and Mathews, F. S. (1999) Detailed active site configuration of a new crystal form of methanol dehydrogenase from *Methylophilus* W3A1 at 1.9 Å resolution. *Biochemistry 38*, 1214−1220.
(35) Zheng, Y. J., Xia, Z., Chen, Z., Mathews, F. S., and Bruice, T. C. (2001) Catalytic mechanism of quinoprotein methanol dehydrogenase: A theoretical and X-ray crystallographic investigation. *Proc. Natl. Acad. Sci. U.S.A. 98*, 432−434.
(36) Lieberman, R. L., Shrestha, D. B., Doan, P. E., Hoffman, B. M., Stemmler, T. L., and Rosenzweig, A. C. (2003) Purified particulate methane monooxygenase from *Methylococcus capsulatus* (Bath) is a dimer with both mononuclear copper and a copper-containing cluster. *Proc. Natl. Acad. Sci. U.S.A. 100*, 3820−3825.
(37) Day, D. J., and Anthony, C. (1990) Methanol dehydrogenase from *Methylobacterium extorquens* AM1. *Methods Enzymol. 188*, 210−216.
(38) Boronowsky, U., Wenk, S. O., Schneider, D., Jäger, C., and Rögner, M. (2001) Isolation of membrane protein subunits in their native state: Evidence for selective binding of chlorophyll and carotenoid to the b_6 subunit of the cytochrome b_6f complex. *Biochim. Biophys. Acta 1506*, 55−66.
(39) Peter, G. F., and Thornber, J. P. (1991) Biochemical composition and organization of higher plant photosystem II light-harvesting pigment-proteins. *J. Biol. Chem. 266*, 16745−16754.
(40) Chistoserdova, L., and Lidstrom, M. E. (1997) Molecular and mutational analysis of a DNA region separating two methylotrophy gene clusters in *Methylobacterium extorquens* AM1. *Microbiology 143*, 1729−1736.
(41) Skovran, E., Palmer, A. D., Rountree, A. M., Good, N. M., and Lidstrom, M. E. (2011) XoxF is required for expression of methanol dehydrogenase in *Methylobacterium extorquens* AM1. *J. Bacteriol. 193*, 6032−6038.
(42) Smith, S. M., Balasubramanian, R., and Rosenzweig, A. C. (2011) Metal reconstitution of particulate methane monooxygenase and heterologous expression of the pmoB subunit. *Methods Enzymol. 495*, 195−210.
(43) Otwinowski, Z., and Minor, W. (1997) Processing of X-ray diffraction data collected in oscillation mode. *Methods Enzymol. 276*, 307−326.
(44) Winter, G. (2010) *xia2*: An expert system for macromolecular crystallography data reduction. *J. Appl. Crystallogr. 43*, 186−190.
(45) Kabsch, W. (2010) Integration, scaling, space-group assignment and post-refinement. *Acta Crystallogr. D66*, 133−144.
(46) Evans, P. R. (2011) An introduction to data reduction: Space-group determination, scaling and intensity statistics. *Acta Crystallogr. D67*, 282−292.
(47) McCoy, A. J., Grosse-Kunstleve, R. W., Adams, P. D., Winn, M. D., Storoni, L. C., and Read, R. J. (2007) Phaser crystallographic software. *J. Appl. Crystallogr. 40*, 658−674.
(48) Winn, M. D., Ballard, C. C., Cowtan, K. D., Dodson, E. J., Emsley, P., Evans, P. R., Keegan, R. M., Krissinel, E. B., Leslie, A. G. W., McCoy, A., McNicholas, S. J., Murshudov, G. N., Pannu, N. S., Potterton, E. A., Powell, H. R., Read, R. J., Vagin, A., and Wilson, K. S. (2011) Overview of the CCP4 suite and current developments. *Acta Crystallogr. D67*, 235−242.
(49) Li, J., Gan, J. H., Mathews, F. S., and Xia, Z. X. (2011) The enzymatic reaction-induced configuration change of the prosthetic group PQQ of methanol dehydrogenase. *Biochem. Biophys. Res. Commun. 406*, 621−626.
(50) Vagin, A. A., Steiner, R. A., Lebedev, A. A., Potterton, L., McNicholas, S., Long, F., and Murshudov, G. N. (2004) REFMAC5 dictionary: Organization of prior chemical knowledge and guidelines for its use. *Acta Crystallogr. D60*, 2184−2195.
(51) Adams, P. D., Afonine, P. V., Bunkoczi, G., Chen, V. B., Davis, I. W., Echols, N., Headd, J. J., Hung, L. W., Kapral, G. J., Grosse-Kunstleve, R. W., McCoy, A. J., Moriarty, N. W., Oeffner, R., Read, R. J., Richardson, D. C., Richardson, J. S., Terwilliger, T. C., and Zwart, P. H. (2010) PHENIX: A comprehensive Python-based system for macromolecular structure solution. *Acta Crystallogr. D66*, 213−221.
(52) Emsley, P., and Cowtan, K. (2004) Coot: Model-building tools for molecular graphics. *Acta Crystallogr. D60*, 2126−2132.
(53) Chen, V. B., Arendall, W. B., Headd, J. J., Keedy, D. A., Immormino, R. M., Kapral, G. J., Murray, L. W., Richardson, J. S., and Richardson, D. C. (2010) MolProbity: All-atom structure validation for macromolecular crystallography. *Acta Crystallogr. D66*, 12−21.
(54) Krissinel, E., and Henrick, K. (2007) Inference of macromolecular assemblies from crystalline state. *J. Mol. Biol. 372*, 774−797.
(55) Adeosun, E. K., Smith, T. J., Hoberg, A. M., Velarde, G., Ford, R., and Dalton, H. (2004) Formaldehyde dehydrogenase preparations from *Methylococcus capsulatus* (Bath) comprise methanol dehydrogenase and methylene tetrahydromethanopterin dehydrogenase. *Microbiology 150*, 707−713.
(56) Zahn, J. A., Bergmann, D. J., Boyd, J. M., Kunz, R. C., and DiSpirito, A. A. (2001) Membrane-associated quinoprotein formaldehyde dehydrogenase from *Methylococcus capsulatus* (Bath). *J. Bacteriol. 183*, 6832−6840.
(57) Folta-Stogniew, E., and Williams, K. R. (1999) Determination of molecular masses of proteins in solution: Implementation of an HPLC size exclusion chromatography and laser light scattering service in a core laboratory. *Journal of Biomolecular Techniques 10*, 51−63.
(58) Anthony, C. (1990) The oxidation of methanol in Gram-negative bacteria. *FEMS Microbiol. Lett. 87*, 209−214.
(59) Chan, H. T. C., and Anthony, C. (1991) The interaction of methanol dehydrogenase and cytochrome c_L in the acidophilic methylotroph *Acetobacter methanolicus*. *Biochem. J. 280*, 139−146.
(60) Cox, J. M., Day, D. J., and Anthony, C. (1992) The interaction of methanol dehydrogenase and its electron acceptor, cytochrome c_L in methylotrophic bacteria. *Biochim. Biophys. Acta 1119*, 97−106.
(61) Pope, C. R., De Feo, C. J., and Unger, V. M. (2013) Cellular distribution of copper to superoxide dismutase involves scaffolding by membranes. *Proc. Natl. Acad. Sci. U.S.A. 110*, 20491−20496.
(62) Stanley, S. H., Prior, S. D., Leak, D. J., and Dalton, H. (1983) Copper stress underlies the fundamental change in intracellular location of methane monooxygenase in methane oxidizing organisms: Studies in batch and continuous cultures. *Biotechnol. Lett. 5*, 487−492.
(63) Prior, S. D., and Dalton, H. (1985) The effect of copper ions on membrane content and methane monooxygenase activity in methanol-grown cells of *Methylococcus capsulatus* (Bath). *J. Gen. Microbiol. 131*, 155−163.